IEEE Access
Multidisciplinary | Rapid Review | Open Access Journal

Received February 19, 2021, accepted March 24, 2021, date of publication March 30, 2021, date of current version April 9, 2021.

Digital Object Identifier 10.1109/ACCESS.2021.3069916

Neuroadaptive Control for Uncertain Euler-Lagrange Systems With Input and Output Constraints

CHANCHAN WANG AND TAI KUANG
Zhejiang College of Security Technology, Wenzhou 325016, China

Corresponding author: Chanchan Wang (chanchanwang2020@163.com)

This work was supported in part by the Project of China Vocational and Technical Education Association under Grant 2020C0525, in part by the Research on the Teaching Reform of Zhejiang Higher Education during the 13th five year plan under Grant jg20191060, and in part by the Project of China Vocational Education Research in Zhejiang Province under Grant ZJCVB35.

ABSTRACT This paper investigates the control issue of Euler-Lagrange systems (ELSs) subject to dynamic uncertainties and external disturbances under input and output constraints, and develops two neuroadaptive control schemes, i.e., direct neuroadaptive approximation method and indirect neuroadaptive approximation method. In the control design, a smooth saturation function called Gaussian error function is used to replace the saturation model, which is applied to solve the input saturation issue. Moreover, a new function is used to guarantee that the output does not violate the restricted boundary. The uncertain dynamic of the ELSs is reconstructed by the direct or indirect neuroadaptive method, and then a virtual-parameter learning method is proposed to reduce the computational load of control schemes. With the aid of Lyapunov stability theory, it is proven that all signals in the closed-loop control system are bounded and the tracking error of ELSs converges to zero under the proposed neuroadaptive control schemes. The simulations on a robotic manipulator illuminate the effectiveness and preponderance of the developed neuroadaptive control schemes.

INDEX TERMS Euler-lagrange system, dynamic uncertainty, input and output constraints, neuroadaptive control.

I. INTRODUCTION

In recent decades, Euler-Lagrange systems (ELSs) have attracted more and more attention from researchers since they can model the dynamics of a large class of physical systems, like surface vehicles [1], [2], robotic manipulators [3], [4], aircrafts [5], underwater vehicles [6], [7], etc. Due to its wide applications in engineering, a rich collection of control schemes can be captured to implement tracking control on the ELSs in existing literature (see, e.g, [**?**], [8], [10] and references therein). In real world applications, the dynamics of ELSs are highly nonlinear and inevitably suffer from parametric and nonparametric uncertainties. Besides, another challenge for the tracking control of ELSs is that these control schemes may fail their goal when the actuator cannot provide adequate power caused by its inherent physical limitations or the system output violates the operational space constraint, i.e., input saturation nonlinearities and output constraints. Hence, referring to the engine control environment, it is significant that the above problems should be stressed elegantly in the control design.

For the uncertain ELSs with parameterized decomposition conditions, the adaptive control schemes [11]–[15], especially the adaptive sliding mode control (SMC) schemes [16], [17], were proposed to ensure the tracking error asymptotical or exponential convergence. In [18], the tracking error asymptotical convergence was also achieved by a recursive robust integral of the sign of the error control method for mechanical servosystems with mismatched uncertainties. In contrast, when the nonparametric uncertainties and external disturbances exist in the ELSs, the control methods mentioned in [11]–[17] are inapplicable. In this context, combining neural network (NN) with adaptive technique, the neuroadaptive control schemes were developed for uncertain robotic manipulators neglecting external disturbances and the issue of operational space constraint [19], [20]. Different from [19], [20], the external disturbance and operational space constraint were taken in account, and [21], [22] employed the

The associate editor coordinating the review of this manuscript and approving it for publication was Valentina E. Balas.

This work is licensed under a Creative Commons Attribution 4.0 License. For more information, see https://creativecommons.org/licenses/by/4.0/

NNs to approximate the lumped unknown nonlinear function vector caused by the unknown dynamic and the external disturbances and the log-type barrier Lyapunov function (BLF) is used to solve the output constraint issue. Similarly, the log-type BLF was also applied to handle the time-varying output constraint of uncertain ELSs in [23], [24]. Based on the concept of BLF, the output constraint problem of surface vehicle [25], [26], underwater robot [27] and robot manipulator [28] was resolved by using the tan-type. Furthermore, the asymmetric BLF (ABLF) was also established to handle the output constraint problem of aircraft [29], surface ship [30], etc. However, a practical factor-input saturation-is not taken into account in the establishment of the closed-loop system in [21]–[29], such an operation may lead to the failure of control objective.

The input saturation is a potential problem for all actuators of control systems, which may lead to unexpected control result or instability. Hence, for the control problem of uncertain ELSs, it is essential to handle the effect of input saturation in the control design. In the literature, several research efforts have been made on the tracking control of ELSs under input saturation. In [31], a finite-time tracking control solution was presented for robot manipulators with actuator saturation, whereas the dynamics of plant were required to be accurately known, and the input saturation effect was not compensated in the control design. Obviously, such a solution is unsuitable for the uncertain ELSs. In [32], an adaptive neural impedance control for uncertain robotic manipulator under input saturation was presented, where an auxiliary dynamic system (ADS) was constructed for compensating the effect of input saturation. Using the same ADS as [32], the tracking control issue of uncertain robotic manipulators under input saturation was resolved under the adaptive neural tracking control scheme [33] and robust adaptive model reference impedance control scheme [34]. Different from the ADS in [32], for the tracking control problem of mechanical systems, [35] adopted the auxiliary filter, whose input is the non-executable part of actuator, to eliminate the input saturation effect. Another method is used a smooth function to replace the saturation model, which is also applied in the tracking control issue of marine surface vehicles [36], [37]. Although the operational space constraint and the inherent physical limitation issue have been fully considered in [21]–[29] and [31]–[37], respectively, these two limitations often exist simultaneously in practice.

Considering both of two limitations, i.e., the constraints both in input and output, several control solutions had been presented for the plants described by ELSs in the existing works. In [38], an auxiliary filter and a log-type BLF were employed to handle the issues of constraints both in input and output for the flexible mechanical systems. [39], [40] presented the fault tolerant control solutions for spacecrafts subject to state constraint and input saturation, where the ADS and tan-type BLF were used to solve the constraints in input and output, respectively. Also, the issue of the constraints both in input and output were taken into account and effectively handled for unmanned surface vessels in [41]. However, the control solution proposed in [41] required the accurate knowledge of ship model. Whereafter, such a requirement was overcome in [42], [43]. Specially, in terms of dealing with the output constraint issue, the BLF-based method was replaced by a constrained transform approach in [43]. Meanwhile, this method was extended to solve the formation control for waterjet unmanned surface vessels under constraints both in input and output in [44]. The work in [45] paid attention to the control issue of the uncertain robot manipulators (RMs) under input saturation and time-varying output constraints, where ADS and ABLF were used to deal with the constraint issues. Although the works in [38]–[45] had presented many meaningful solutions to the plants described by ELSs, these control solutions can only guarantee that the tracking error of the plants is bounded, i.e., the zero tracking error cannot be obtained. Further research on the zero tracking error of the uncertain ELSs simultaneously with input and output constraints brings forward the challenge.

Inspired by the above-mentioned discussion, this paper attempts to develop two neuroadaptive control schemes for uncertain ELSs simultaneously with input and output constraints. In the control design, a smooth function is applied to replace the non-smooth nonlinearly. Furthermore, the Nussbaum function is introduced to handle the issue of time-varying gain caused by the smooth function. For the output constrain issue, this work discards the BLF used in [21], [22], [26], [43], which is replace by a new function. In addition, RBF NNs are applied to approximate the unknown nonlinear function vector caused by the uncertain dynamic, directly. And then, in the combination with virtual parametric technology, a direct neuroadaptive control scheme is developed. Moreover, in the second scheme, a RBF NNs is applied to approximate the norm of unknown nonlinear function vector. In this context, a indirect neuroadaptive control scheme is developed. The main contributions of this work can be summarized as:

1) Compared with the works [21]–[29] and [31]–[37], where [21]–[29] take the output constraint issue account into the control design and [31]–[37] take the input saturation issue account into the control design, the proposed neuroadaptive control schemes can simultaneously solve constrains both input and output for uncertain ELSs, and guarantees that the constrains both input and output are not violated.
2) Compared with the works [21]–[22], [32]–[33] and [41], where a number of adaptive regressors are employed to update the unknown ideal weight, only one unknown parameter needs to be learned online under the proposed direct/indirect neuroadaptive control schemes. As a result, the computational load is greatly reduced.
3) Compared with the works [38]–[45], which can only guarantee the boundedness of the output tracking error of plants, the proposed direct/indirect neuroadaptive

control schemes guarantee that the tracking error converge to zero as $t \to \infty$.

This paper is organized as follows. Sections 2 address the problem formulation and preliminaries. Section 3 presents the control design process and the stability analysis. Section 4 provides the simulation results. Section 5 draws the conclusions.

Notations: In this paper, $||\cdot||$ represents the 2-norm of a matrix or vector. $\lambda_{min}(\cdot)$ represent the minimum eigenvalue of a matrix. sgn$(\cdot)$ is the sign function. $\tilde{(\cdot)} = (\cdot) - \hat{(\cdot)}$ denotes the error between the unknown parameter $(\cdot)$ and its estimate value $\hat{(\cdot)}$.

II. PROBLEM FORMULATION AND PRELIMINARIES

A. PROBLEM FORMULATION

In general, the ELSs with the second-order dynamics can be described as follows:

$$\boldsymbol{M}(\boldsymbol{q})\ddot{\boldsymbol{q}} + \boldsymbol{C}(\boldsymbol{q}, \dot{\boldsymbol{q}})\dot{\boldsymbol{q}} + \boldsymbol{G}(\boldsymbol{q}) + \boldsymbol{F}(\boldsymbol{q}, \dot{\boldsymbol{q}}) = \boldsymbol{\tau} + \boldsymbol{\tau_d} \tag{1}$$

where $\boldsymbol{q}$, $\boldsymbol{q}$ and $\dot{\boldsymbol{q}} \in R^n$ denote the position, velocity and acceleration of Lagrangian coordinates. $\boldsymbol{M}(\boldsymbol{q})$, $\boldsymbol{C}(\boldsymbol{q}, \dot{\boldsymbol{q}})$, $\boldsymbol{G}(\boldsymbol{q})$ and $\boldsymbol{F}(\boldsymbol{q}, \dot{\boldsymbol{q}})$ denote the inertial matrix, the matrix of Coriolis and centripetal matrix, the gravity vector, and the friction vector, respectively. $\boldsymbol{\tau}_d = [\tau_{d,1}, \cdots, \tau_{d,n}]^T$ denotes the external disturbance vector and $\boldsymbol{\tau} = [\tau_1, \cdots, \tau_n]^T$ is the control input vector. In practice, due to the physical limits of the actuator, the input saturation nonlinearity can be expressed by

$$\tau_i = \begin{cases} \text{sgn}(\tau_{i,c})\tau_{i,m}, & \text{if} \quad \tau_{i,c} > \tau_{i,m} \\ \tau_{i,c}, & \text{if} \quad \tau_{i,c} < \tau_{i,m} \end{cases} \quad i = 1, \cdots, n \tag{2}$$

where $\tau_c = [\tau_{1,c}, \cdots, \tau_{n,c}]^T$ denotes the command control vector calculated by the control law and $\tau_{i,m} > 0$ represents the maximum control input provided by the ith actuator. Considering the safe operation, the output of system (1) are subject to $|q_{1,i}| < \kappa_{c,i}$, $i = 1, \cdots, n$, where $\kappa_{c,i}$ is the constraint boundary of ith component of the system output.

In this work, we make the following standard assumptions:

Assumption 1: $\boldsymbol{\tau_d}$ is bounded, that is, $||\boldsymbol{\tau_d}|| \leq \bar{\tau}_d$ with $\bar{\tau}_d > 0$ being an unknown constant.

Assumption 2: The matrixes $\boldsymbol{M}(\boldsymbol{q})$, $\boldsymbol{C}(\boldsymbol{q}, \dot{\boldsymbol{q}})$, $\boldsymbol{G}(\boldsymbol{q})$ and $\boldsymbol{F}(\boldsymbol{q}, \dot{\boldsymbol{q}})$ are completely unknown.

Assumption 3: The desired trajectory $\boldsymbol{q_d} = [q_{d,1}, \cdots, q_{d,n}]^T$, and its first and second order derivatives are bounded. In addition, $q_{d,i}$ satisfies $|q_{d,i}| \leq \kappa_{d,i} < \kappa_{c,i}$ with $\kappa_{d,i}$ being known positive constants.

The control objective of this paper is to design a robust adaptive NN tracking control law $\boldsymbol{\tau_c}$ for the uncertain EL system (1) subject to input and output constraints under Assumptions 1-3 such that the output $\boldsymbol{q}$ of the system (1) tracks the desired trajectory $\boldsymbol{q_d}$, and the output constraints are never violated (i.e. $|q_{1,i}| < \kappa_{c,i}$, for $\forall t \geq 0$). Meanwhile, all signals in the closed-loop control system are bounded.

From (2), τ_i is a non-smooth function with respect to $\tau_{i,c}$, $i = 1, \cdots, n$, and is featured by a non-smooth nonlinearity. Here, the saturation function defined in (2) is replaced by the following function:

$$\xi_i(\tau_{i,c}) = \tau_{i,m}\mathcal{F}\left(\frac{\sqrt{\pi}\tau_{i,c}}{2\tau_{i,m}}\right) \tag{3}$$

where $\mathcal{F}(\cdot)$ is a Gaussian error function defined as $\mathcal{F}(\jmath) = \frac{2}{\sqrt{\pi}}\int_0^{\jmath} e^{-\iota^2} d\jmath$. In view of (2) and (3), one can get

$$\tau_i(\tau_{i,c}) = \xi_i(\tau_{i,c}) + \epsilon_i(\tau_{i,c}) \tag{4}$$

where $\text{æ}_i(\tau_{i,c})$ is approximation error satisfying $|\epsilon_i(\tau_{i,c})| = |\tau_i(\tau_{i,c}) - \xi_i(\tau_{i,c})| \leq E_{i,m}$ with $E_{i,m} \in R^+$.

Utilizing the mean-value theorem, $\xi_i(\tau_{i,c})$ is rewritten as

$$\xi_i(\tau_{i,c}) = \xi_i(\tau'_{i,c}) + \varrho_i(\tau_{i,c} - \tau'_{i,c}) \tag{5}$$

where $\varrho_i = \exp\left(-\left(\frac{\sqrt{\pi}\tau^l_{i,c}}{2\tau_{i,m}}\right)^2\right)$ and $\tau^l_{i,c} = \iota\tau_{i,c} + (1-\iota)\tau^*_{i,c}$ with $\iota \in (0, 1)$. Let $\tau'_{i,c} = 0$, and then we have

$$\tau_i(\tau_{i,c}) = \varrho_i\tau_{i,c} + \epsilon_i(\tau_{i,c}) \tag{6}$$

Remark 1: From the expression of ϱ_i, we know that ξ_i is a non-increasing function, that is, ϱ_i is bounded and satisfies $\varrho_i \in (0, 1]$ for $\forall\tau_{i,c} \in R$. In addition, according to $|\epsilon_i(\tau_{i,c})| \leq E_{i,m}$, $||\boldsymbol{E}(\boldsymbol{\tau}_c)|| \leq E_\epsilon$ holds, where $\boldsymbol{E}(\boldsymbol{\tau}_c) = [\epsilon_1(\tau_{1,c}), \cdots, \epsilon_3(\tau_{n,c})]^T$ and E_ϵ is a positive constant.

In the light of Eqs.(1) and (6), we have

$$\boldsymbol{M}(\boldsymbol{q})\ddot{\boldsymbol{q}} + \boldsymbol{C}(\boldsymbol{q}, \dot{\boldsymbol{q}})\dot{\boldsymbol{q}} + \boldsymbol{G}(\boldsymbol{q}) + \boldsymbol{F}(\boldsymbol{q}, \dot{\boldsymbol{q}}) = \boldsymbol{\varrho}\boldsymbol{\tau}_c + \boldsymbol{\tau_\epsilon} \tag{7}$$

where $\boldsymbol{\varrho} = diag(\varrho_1, \cdots, \varrho_n)$ and $\boldsymbol{\tau_\epsilon} = \boldsymbol{\tau_d} + \boldsymbol{\epsilon}$. According to Assumption 1 and $||\boldsymbol{E}(\boldsymbol{\tau}_c)|| \leq E_\epsilon$, $||\boldsymbol{\tau_\epsilon}|| \leq \bar{d}$ with $\bar{d} > 0$ being an unknown constant.

B. PRELIMINARIES

Definition 1 [46]: For any continuous function $N(\zeta) : R \to R$, the function is a Nussbaum function if it has the following properties:

$$\lim_{t\to\infty} \sup \frac{1}{s}\int_0^s N(\zeta)d\zeta = +\infty \tag{8}$$

$$\lim_{t\to\infty} \inf \frac{1}{s}\int_0^s N(\zeta)d\zeta = -\infty \tag{9}$$

In existing literature, commonly used Nussbaum functions include $\zeta^2\cos(\zeta)$, $e^{\zeta^2}\cos\left(\frac{\pi}{2}\zeta\right)$, $\zeta^2\sin(\zeta)$, etc. In this work, we choose the Nussbaum function as $\zeta^2\cos(\zeta)$.

Lemma 1: [46], [47] Let $V(\cdot)$ and $\zeta(\cdot)$ be smooth functions defined on $[0, t_f)$ with $V(t) \geq 0$, $\forall t \in [0, t_f)$, and $N(\cdot)$ is an even Nussbaum-type function. If the following inequality holds

$$V(t) \leq c_0 + e^{-\iota t}\int_0^t (g(\jmath)N(\zeta(\jmath)) + 1)\dot{\zeta}(\jmath)e^{\iota\jmath}d\jmath, \quad \forall t \in [0, t_f) \tag{10}$$

where c_0 is a suitable constant, $\iota > 0$ is a constant and $g(\jmath)$ is a time-varying parameter which takes the value in the unknown interval $\Pi = [f^-, f^+]$ with $0 \notin \Pi$. Then, $\zeta(t)$, $V(t)$ and $\int_0^t g(\jmath)N(\zeta(\jmath) + 1)\dot{\zeta}(\jmath)d\jmath$ must be bounded on $[0, t_f)$.

Lemma 2: [48], [49] Let $\boldsymbol{A}$ be a $n \times n$ symmetric matrix, and $\boldsymbol{y} \in R^n$ be a nonzero vector, denote that $a = \frac{\boldsymbol{y}^T\boldsymbol{A}\boldsymbol{y}}{\boldsymbol{y}^T\boldsymbol{y}}$. Then, there exists at least one eigenvalue of $\boldsymbol{A}$ in the internal $(-\infty, a]$ and at least one in $[a, \infty)$.

Lemma 3: [48], [49] Any real matrix can be expressed as the sum of a symmetric matrix and a skew ones.

Lemma 4: [50] For any $x \in R$ and $y \in R$, the following inequality holds

$$xy \leq \frac{m^p}{p}|x|^p + \frac{1}{m^q q}|y|^q \tag{11}$$

where $m > 0$, $p > 1$ and $q > 1$ are constants that satisfy $(p-1)(q-1) = 1$.

Lemma 5: [36], [43] For a nonlinear function $\varphi(\boldsymbol{Z}) : R^n \to R$ defined on a compact set $\boldsymbol{Z} \subset \Omega_Z \in R^n$, there exists a radial basis function NN $\boldsymbol{\vartheta}^{*T}\boldsymbol{\beta}(\boldsymbol{Z})$ such that the following equation holds

$$\varphi(\boldsymbol{Z}) = \boldsymbol{\vartheta}^{*T}\boldsymbol{\beta}(\boldsymbol{Z}) + \varepsilon \tag{12}$$

where approximate error ε satisfies $|\varepsilon| \leq \varepsilon^*$ with $\varepsilon^* > 0$ being constant, $\boldsymbol{\beta}(\boldsymbol{Z}) = [\beta_1(\boldsymbol{Z}), \cdots, \beta_\ell(\boldsymbol{Z})]^T$ is the basis function vector, $\boldsymbol{\vartheta}^* = [\vartheta_1^*, \cdots, \vartheta_\ell^*]^T$ is the ideal weight vector, and $\ell > 1$ is the node number. The basis function $\xi_i(Z)$, $i = 1, \cdots, \ell$, is the Gaussian function, that is,

$$\beta_i(\boldsymbol{Z}) = \exp\left[-\frac{(\boldsymbol{Z}-\boldsymbol{c}_i)^T(\boldsymbol{Z}-\boldsymbol{c}_i)}{\sigma_i^2}\right] \tag{13}$$

with $\boldsymbol{c}_i = [c_{i,1}, \cdots, c_{i,\ell}]^T$ and σ_i being the receptive field's center and the width of basis function.

Lemma 6: For any scalar $\kappa \in R_+$ and $z \in R$, the following inequality holds in the interval $|z| < \kappa$:

$$\log\frac{\kappa^2}{\kappa^2 - z^2} \leq \frac{1}{2}\left(\frac{\kappa z}{\kappa^2 - z^2}\right)^2 \tag{14}$$

Proof: Please see Appendix A.

III. CONTROL DESIGN FOR STATIC CONSTRAINT

In this section, two adaptive neural tracking control laws are designed to solve the tracking control problem of uncertain ELSs subject to static output constraint and input saturation, in which one is the direct approximation method and the other one is the indirect approximation method. In addition, we also present the detailed stability analysis utilizing the Lyapunov stability theory for the Euler-Lagrange closed-loop tracking control system.

Let $\boldsymbol{x_1} = \boldsymbol{q}$ and $\boldsymbol{x_2} = \dot{\boldsymbol{q}}$. Then, Eq.(7) can be rewritten as

$$\begin{cases} \dot{\boldsymbol{x}}_1 = \boldsymbol{x}_2 \\ \dot{\boldsymbol{x}}_2 = \boldsymbol{f}(\boldsymbol{x}) + \boldsymbol{g}(\boldsymbol{x})\boldsymbol{\varrho}\boldsymbol{\tau}_c + \boldsymbol{d}_{\boldsymbol{x}} \end{cases} \tag{15}$$

where $\boldsymbol{x} = [\boldsymbol{x_1}^T, \boldsymbol{x_2}^T]^T$, $\boldsymbol{f}(\boldsymbol{x}) = -\boldsymbol{M}^{-1}(\boldsymbol{x_1})\Big(\boldsymbol{C}(\boldsymbol{x_1}, \boldsymbol{x_2})\boldsymbol{x_2} + \boldsymbol{G}(\boldsymbol{x_1}) + \boldsymbol{F}(\boldsymbol{x_1}, \boldsymbol{x_2})\Big)$, $\boldsymbol{g}(\boldsymbol{x}) = \boldsymbol{M}^{-1}(\boldsymbol{x_1})$ and $\boldsymbol{d}_{\boldsymbol{x}} = \boldsymbol{M}^{-1}(\boldsymbol{x_1})\boldsymbol{\tau}_{\boldsymbol{\epsilon}}$.

According to Remark 1, there exists unknown constant ϱ_0 satisfying $0 < \varrho_0 \leq \lambda_{min}(\boldsymbol{\varrho})$. Further, note that $\boldsymbol{M}(\boldsymbol{q})$ is a symmetric and positive-definite matrix, so is $\boldsymbol{M}^{-1}(\boldsymbol{q})$. Then, all eigenvalues of the gain matrix $\boldsymbol{g}(\boldsymbol{x})\boldsymbol{\varrho}$ are positive. It should be pointed that $\boldsymbol{g}(\boldsymbol{x})\boldsymbol{\varrho}$ is asymmetric. With Lemma 3, $\bar{\boldsymbol{g}}(\boldsymbol{x}) = \boldsymbol{g}(\boldsymbol{x})\boldsymbol{\varrho}$ can be decomposed as

$$\bar{\boldsymbol{g}}(\boldsymbol{x}) = \bar{\boldsymbol{g}}_{\boldsymbol{1}}(\boldsymbol{x}) + \bar{\boldsymbol{g}}_{\boldsymbol{2}}(\boldsymbol{x}) \tag{16}$$

where matrices $\boldsymbol{g}_1(\boldsymbol{x}) = \frac{1}{2}(\bar{\boldsymbol{g}}^T(\boldsymbol{x}) + \bar{\boldsymbol{g}}(\boldsymbol{x}))$ and $\bar{\boldsymbol{g}}_{\boldsymbol{2}}(\boldsymbol{x}) = \frac{1}{2}(-\bar{\boldsymbol{g}}^T(\boldsymbol{x}) + \bar{\boldsymbol{g}}(\boldsymbol{x}))$ are symmetric and skew-symmetric. Further, from Lemma 2, for any given non-zero vector $\boldsymbol{y} \in R^n$, we have

$$\boldsymbol{y}^T\bar{\boldsymbol{g}}(\boldsymbol{x})\boldsymbol{y} = \boldsymbol{y}^T\left(\bar{\boldsymbol{g}}_{\boldsymbol{1}}(\boldsymbol{x}) + \bar{\boldsymbol{g}}_{\boldsymbol{2}}(\boldsymbol{x})\right)\boldsymbol{y} = \boldsymbol{y}^T\bar{\boldsymbol{g}}_{\boldsymbol{1}}(\boldsymbol{x})\boldsymbol{y} \tag{17}$$

Then, we obtain

$$\boldsymbol{y}^T\bar{\boldsymbol{g}}(\boldsymbol{x})\boldsymbol{y} = a(t)\boldsymbol{y}^T\boldsymbol{y} \tag{18}$$

with $a(t) > 0$. Recalling the property of $\bar{\boldsymbol{g}}(\boldsymbol{x})$ and Lemma 2, there exist positive constants a_1 and a_2 such that $a_1 \leq a(t) \leq a_2$.

Remark 2: From (16)-(18), the control problem of uncertain nonlinear systems with the asymmetric gain $\boldsymbol{g}(\boldsymbol{x})\boldsymbol{\varrho}$ has been transformed into that one with a time-varying control gain $a(t)$, equivalently. However, in the control design and analysis, the biggest obstacle is how to deal with time-varying control gain $a(t)$. In this context, inspired by [46] a powerful tool, i.e., Nussbaum-type function, is employed to overcome the obstacle.

Define the tracking error vector $\boldsymbol{e_1} = \boldsymbol{x_1} - \boldsymbol{x_d}$ with $\boldsymbol{x_d} = \boldsymbol{q_d}$. Further, we have $\boldsymbol{e_2} = \dot{\boldsymbol{e}}_{\boldsymbol{1}} = \dot{\boldsymbol{x}}_{\boldsymbol{1}} - \dot{\boldsymbol{x}}_{\boldsymbol{d}}$ from (1). Furthermore, introduce the new variable $\boldsymbol{\chi} \in R^n$ to implement the transformation of output constraint as follows

$$\boldsymbol{\chi} = \boldsymbol{e_2} + \boldsymbol{\psi}(\boldsymbol{e_1})\boldsymbol{e_1} \tag{19}$$

where

$$\boldsymbol{\psi}(\boldsymbol{e_1}) = diag\left(\frac{\delta_1}{\kappa_1^2 - e_{1,1}^2}, \cdots, \frac{\delta_n}{\kappa_n^2 - e_{1,n}^2}\right) \tag{20}$$

with δ_i, $i = 1, \cdots, n$, being a design constant and κ_i being the bound of tracking error $e_{1,i}$. According to the condition of output constraint $|q_{1,i}| < \kappa_{c,i}$ and Assumption 3, κ_i can be calculated as

$$\kappa_i = \kappa_{c,i} - \kappa_{d,i} \tag{21}$$

Lemma 7: If $|q_{1,i}(0)| < \kappa_{c,i}$ holds $\forall i$ and the boundedness of $\boldsymbol{\chi}$ is ensured for $\forall t \geq 0$, the constraint condition $|q_{1,i}| < \kappa_{c,i}$ will never be violated.

Proof: Please see Appendix B.

The time-derivative of $\boldsymbol{\chi}$ is given by

$$\dot{\boldsymbol{\chi}} = \dot{\boldsymbol{e}}_{\boldsymbol{2}} + \breve{\boldsymbol{\psi}}(\boldsymbol{e_1})\dot{\boldsymbol{e}}_{\boldsymbol{1}} \tag{22}$$

where

$$\breve{\boldsymbol{\psi}}(\boldsymbol{e_1}) = diag\left(\frac{\delta_1(\kappa_1^2 + e_{1,1}^2)}{(\kappa_1^2 - e_{1,1}^2)^2}, \cdots, \frac{\delta_n(\kappa_n^2 + e_{1,n}^2)}{(\kappa_n^2 - e_{1,n}^2)^2}\right) \tag{23}$$

Using $\boldsymbol{e_2} = \dot{\boldsymbol{x}}_{\boldsymbol{1}} - \dot{\boldsymbol{x}}_{\boldsymbol{d}}$ and Eq. (15), Eq.(21) can be rewritten as

$$\dot{\boldsymbol{\chi}} = \boldsymbol{f}(\boldsymbol{x}) + \boldsymbol{g}(\boldsymbol{x})\boldsymbol{\varrho}\boldsymbol{\tau}_c + \boldsymbol{d}_{\boldsymbol{x}} - \ddot{\boldsymbol{x}}_{\boldsymbol{d}} + \breve{\boldsymbol{\psi}}(\boldsymbol{e_1})\boldsymbol{e_2} \tag{24}$$

A. DIRECT APPROXIMATION METHOD

In the view of Assumption 2, $\boldsymbol{f}(\boldsymbol{x}) \in R^n$ is unknown. Considering Lemma 5, $\boldsymbol{f}(\boldsymbol{x})$ can be approximated using RBF NN, and then we have

$$\boldsymbol{f}(\boldsymbol{x}) = \boldsymbol{\vartheta}^{*T}\boldsymbol{\beta}(\boldsymbol{x}) + \boldsymbol{\varepsilon} \tag{25}$$

where $\boldsymbol{\varepsilon} \in R^n$ satisfies $||\boldsymbol{\varepsilon}|| \leq \bar{\varepsilon}$ with $\bar{\varepsilon} \geq$ being a constant, $\boldsymbol{\vartheta}^* = diag(\boldsymbol{\vartheta}_1^{*T}, \cdots, \boldsymbol{\vartheta}_n^{*T})$ with $\boldsymbol{\vartheta}_i^* = [\vartheta_{i,1}^*, \cdots, \vartheta_{i,\ell}^*]^T$ is the ideal weight matrix, and $\boldsymbol{\beta}(\boldsymbol{x}) = [\boldsymbol{\beta}_1(\boldsymbol{x}), \cdots, \boldsymbol{\beta}_n(\boldsymbol{x})]^T$ with $\boldsymbol{\beta}_i(\boldsymbol{x}) = [\beta_{i,1}(\boldsymbol{x}), \cdots, \beta_{i,\ell}(\boldsymbol{x})]^T$ is the basis function vector of NNs. Further, according to $||\boldsymbol{\tau}|| \leq \bar{d}$ and the property of $\boldsymbol{M}(\boldsymbol{q})$ [37], there exists an unknown positive constant d_τ satisfying $||\boldsymbol{d_x}|| \leq d_\tau$. In addition, considering Assumption 3, we have $||\boldsymbol{\varepsilon} + \boldsymbol{d_x} - \ddot{\boldsymbol{x}}_{\boldsymbol{d}}|| \leq d_x$ with d_x being an unknown positive constant.

Let $\bar{\boldsymbol{f}}(\boldsymbol{Z}) = \boldsymbol{f}(\boldsymbol{x}) + \boldsymbol{d_x} - \ddot{\boldsymbol{x}}_{\boldsymbol{d}} + \breve{\boldsymbol{\psi}}(\boldsymbol{e_1})\boldsymbol{e_2}$ with $\boldsymbol{Z} = [\boldsymbol{x}^T, \boldsymbol{e_1}^T, \boldsymbol{e_2}^T]^T$. Taking the following transformation for $\bar{\boldsymbol{f}}(\boldsymbol{Z})$ yields

$$\begin{aligned} ||\bar{\boldsymbol{f}}(\boldsymbol{Z})|| &\leq ||\boldsymbol{\vartheta}^*||||\boldsymbol{\beta}(\boldsymbol{x})|| + ||\breve{\boldsymbol{\psi}}(\boldsymbol{e_1})\boldsymbol{e_2}|| + ||\boldsymbol{\varepsilon} + \boldsymbol{d_x} - \ddot{\boldsymbol{x}}_{\boldsymbol{d}}|| \\ &\leq \Theta\varsigma(\boldsymbol{Z}) \end{aligned} \tag{26}$$

where $\varsigma(\boldsymbol{Z}) = ||\boldsymbol{\beta}(\boldsymbol{x})|| + ||\breve{\boldsymbol{\psi}}(\boldsymbol{e_1})\boldsymbol{e_2}|| + 1$ and $\Theta = \max\{||\boldsymbol{\vartheta}^*||, ||\boldsymbol{\varepsilon} + \boldsymbol{d_x} - \ddot{\boldsymbol{x}}_{\boldsymbol{d}}||, 1\}$.

Remark 3: In $\Theta = \max\{||\boldsymbol{\vartheta}^*||, ||\boldsymbol{\varepsilon} + \boldsymbol{d_x} - \ddot{\boldsymbol{x}}_{\boldsymbol{d}}||, 1\}$, $||\boldsymbol{\vartheta}^*||$ is the norm of the ideal weight matrix, which is not of the clear physical significance. Similarly, $||\boldsymbol{\varepsilon} + \boldsymbol{d_x} - \ddot{\boldsymbol{x}}_{\boldsymbol{d}}||$ is not of the clear physical significance even if $\ddot{\boldsymbol{x}}_{\boldsymbol{d}}$ has a clear physical significance. Therefore, the unknown constant Θ is also not of the clear physical significance. Here, Θ is called *virtual parameter*. By utilizing online learning method, the estimation of Θ can be obtained, which is called *virtual-parameter learning* technique.

Synthesizing Eqs.(24) and (26), one can get

$$\boldsymbol{\chi}^T\dot{\boldsymbol{\chi}} \leq \boldsymbol{\chi}^T\boldsymbol{g}(\boldsymbol{x})\boldsymbol{\varrho}\boldsymbol{\tau}_c + \Theta||\boldsymbol{\chi}||\varsigma(\boldsymbol{Z}) \tag{27}$$

Using Lemma 4, we have

$$\Theta||\boldsymbol{\chi}||\varsigma(\boldsymbol{Z}) \leq \Theta||\boldsymbol{\chi}||^2\varsigma^2(\boldsymbol{Z}) + \frac{\Theta}{4} \tag{28}$$

Substituting Eq.(28) into Eq. (27) yields

$$\boldsymbol{\chi}^T\dot{\boldsymbol{\chi}} \leq \boldsymbol{\chi}^T\Big(\boldsymbol{g}(\boldsymbol{x})\boldsymbol{\varrho}\boldsymbol{\tau}_c + \Theta\boldsymbol{\chi}\varsigma^2(\boldsymbol{Z})\Big) + \frac{\Theta+1}{4} \tag{29}$$

Design the control law for ELSs (1) as follows

$$\boldsymbol{\tau}_c = N(\boldsymbol{\zeta})\eta\boldsymbol{\chi} \tag{30}$$

$$\dot{\boldsymbol{\zeta}} = \boldsymbol{\chi}^T\boldsymbol{\chi}\eta \tag{31}$$

$$\eta = k + \hat{\Theta}\varsigma^2(\boldsymbol{Z}) \tag{32}$$

$$\dot{\hat{\Theta}} = \rho\boldsymbol{\chi}^T\boldsymbol{\chi}\varsigma^2(\boldsymbol{Z}) - \sigma\hat{\Theta} \tag{33}$$

where $k > 0$, $\rho > 0$ and $\sigma > 0$ are design constants and $\zeta \in R$ is the Nussbaum variable.

Consider the following Lyapunov function

$$V = \frac{1}{2}\boldsymbol{\chi}^T\boldsymbol{\chi} + \frac{1}{2\rho}\tilde{\Theta}^2 \tag{34}$$

Taking the time-derivative of V, and using Eqs. (18), (30) and (31), one can obtain

$$\begin{aligned} \dot{V} &\leq N(\zeta)\eta\boldsymbol{\chi}^T\boldsymbol{g}(\boldsymbol{x})\boldsymbol{\varrho}\boldsymbol{\chi} + \boldsymbol{\chi}^T\Theta\boldsymbol{\chi}\varsigma^2(\boldsymbol{Z}) + \frac{\Theta+1}{4} - \frac{1}{\rho}\tilde{\Theta}\dot{\hat{\Theta}} \\ &= \Big(N(\zeta)a(t)+1\Big)\dot{\zeta} - k\boldsymbol{\chi}^T\boldsymbol{\chi} + \frac{\sigma}{\rho}\tilde{\Theta}\hat{\Theta} + \frac{\Theta+1}{4} \\ &\leq \Big(N(\zeta)a(t)+1\Big)\dot{\zeta} - k\boldsymbol{\chi}^T\boldsymbol{\chi} - \frac{\sigma}{2\rho}\tilde{\Theta}^2 + \frac{\sigma}{2\rho}\Theta^2 + \frac{\Theta+1}{4} \\ &= -cV + \Big(N(\zeta)a(t)+1\Big)\dot{\zeta} + d \end{aligned} \tag{35}$$

where $c = \min\{2k, \sigma\}$ and $d = \frac{\sigma}{2\rho}\Theta^2 + \frac{\Theta+1}{4}$.

Solving Eq.(35) yields

$$V(t) \leq \frac{d}{c} + V(0) + e^{-ct}\int_0^t \Big(N(\zeta)a(t_\iota)+1\Big)\dot{\zeta}e^{ct_\iota}dt_\iota \tag{36}$$

where $V(0)$ is the initial value of $V(t)$.

Based on the above analysis, the main results are given by the following theorem.

Theorem 1: Consider the uncertain ELSs (1) under Assumptions 1-3, if the initial condition of q satisfies $|q_{1,i}(0)| < \kappa_{c,i}$ for $\forall i$, then the designed control law (30) with the adaptive laws (31) and (33) is able to make the following properties hold

1) All signals in the closed-loop tracking control system are bounded.
2) The output $\boldsymbol{q}$ of ELSs (1) will never violate the output constraint condition, i.e., $|q_{1,i}| < \kappa_{c,i}$, $\forall i \in \{1, \cdots, n\}$.

Zero-error

3) tracking control is achieved, i.e., $\boldsymbol{e_1} \to 0$ as $t \to 0$.

Proof: 1) Boundedness of all signals. According to Lemma 1 and Eq.(36), $V(t)$, $\zeta(t)$ and $\int_0^t \Big(N(\zeta)a(t_\iota)+1\Big)\dot{\zeta}dt_\iota$ are bounded if $|q_{1,i}(0)| < \kappa_{c,i}$ for $\forall i$. Further, $\boldsymbol{\chi}$ and $\tilde{\Theta}$ are also bounded from (34), and $\hat{\Theta}$ is also bounded due to $\tilde{\Theta} = \Theta - \hat{\Theta}$. In addition, considering Eq. (33) and the boundedness of $\hat{\Theta}$ and χ, $\varsigma(\boldsymbol{x})$ is also bounded. Furthermore, $\boldsymbol{\tau_c}$ is also bounded. From Lemma 6 and the boundedness of $\boldsymbol{\chi}$, $\boldsymbol{e_1}$ is bounded and $|e_{1,i}| < \kappa_i$. Further, $\boldsymbol{e_2}$ is bounded from Eq. (18). Therefore, all signals in the closed-loop tracking control system are bounded. Recalling Lemma 6, the output constraint condition $|q_{1,i}| < \kappa_{c,i}$ always holds.

2) Uniform continuity of all signals. According to (30), we have

$$\begin{aligned} \dot{\boldsymbol{\tau}}_c = &\frac{\partial\boldsymbol{\tau}_c}{\partial\eta}\frac{\partial\eta}{\partial\hat{\Theta}}\dot{\hat{\Theta}} + \frac{\partial\boldsymbol{\tau}_c}{\partial\eta}\frac{\partial\eta}{\partial\varsigma(\boldsymbol{Z})}\frac{\partial\varsigma(\boldsymbol{Z})}{\partial\boldsymbol{Z}}\dot{\boldsymbol{Z}} \\ &+ \frac{\partial\boldsymbol{\tau}_c}{\partial N(\boldsymbol{\zeta})}\frac{\partial N(\boldsymbol{\zeta})}{\partial\boldsymbol{\zeta}}\dot{\boldsymbol{\zeta}} + \frac{\partial\boldsymbol{\tau}_c}{\partial\boldsymbol{\chi}}\dot{\boldsymbol{\chi}} \end{aligned} \tag{37}$$

Owing to (3)*, the actual control input* $\boldsymbol{\tau}$ *is continuous and bounded. Moreover, from the boundedness of* $\boldsymbol{d_x}$ $\boldsymbol{e_1}$, $\boldsymbol{e_2}$ *and* $\boldsymbol{\tau_c}$*, the boundedess of* $\dot{\boldsymbol{x}}_{\boldsymbol{2}}$ *can be determined, together with Assumption 3,*(22) *and* (37)*,* $\dot{\boldsymbol{Z}}$ *and* $\dot{\boldsymbol{\chi}}$ *are continuous and bounded. Furthermore, according to (33) and (35), we can obtain that* $\dot{\hat{\Theta}}$ *and* $\dot{\boldsymbol{\zeta}}$ *are continuous and bounded. Therefore,* $\dot{\boldsymbol{\tau}}_c$ *is also continuous and bounded, i.e., all signals in the closed-loop control system are uniformly continuous.*

3) convergence of tracking erroes. According to Eqs.(31) and (32), one can obtain $\dot{\zeta} = \boldsymbol{\chi}^T\boldsymbol{\chi}(k + \hat{\Theta}\varsigma^2(\boldsymbol{Z})) \geq k\boldsymbol{\chi}^T\boldsymbol{\chi}$. Furthermore, $k\int_0^t \boldsymbol{\chi}^T\boldsymbol{\chi} \leq \zeta(t) - \zeta(0)$. Due to the boundedness of $\zeta(t)$, $\boldsymbol{\chi} \in L_2$. In addition, $\boldsymbol{\chi}$ is bounded, then $\boldsymbol{\chi} \in L_2 \cap L_\infty$. Using Barbalat Lemma, we can get $\boldsymbol{\chi} \to 0$ as $t \to \infty$. Furthermore, recalling Eq.(60), we can get $V_{\boldsymbol{e}} = \frac{\boldsymbol{\chi}^T\boldsymbol{\chi}}{16\rho} + \left(V_{\boldsymbol{e}}(0) - \frac{\boldsymbol{\chi}^T\boldsymbol{\chi}}{16\rho}\right)e^{-4\rho t}$. Hence, $\boldsymbol{\chi} \to 0$ as $t \to \infty$, $V_{\boldsymbol{e}} \to \infty$, that is, $\log\left(\frac{\kappa_i^2}{\kappa_i^2 - e_{1,i}^2}\right) \to 0$, which indicates that $e_{i,1} \to 0$ can be achieved. Therefore, zero-error tracking control is achieved.

Remark 4: From Eq.(24), to reconstruct the unknown nonlinear function vector $\boldsymbol{f}(\boldsymbol{x})$, n RBF NNs are involved. Although through the transformation (26), only one unknown parameter Θ needs to be updated online, the heavy computational burden is still not completely lifted due to the use of multiple RBF NNs. In order to solve the problem, we adopt the indirect approximation method, in which only one RBF NN is applied to handle the unknown nonlinear function vector $\boldsymbol{f}(\boldsymbol{x})$.

B. INDIRECT APPROXIMATION METHOD

In this subsection, the indirect approximation method is used to reduce the heavy computational burden of control law (30).

Recalling Eq.(23), $\boldsymbol{f}(\boldsymbol{x}) \in R^n$ is unknown. Here, let $L(\boldsymbol{x}) = ||\boldsymbol{f}(\boldsymbol{x})||$, which can be approximated by a RBF NN, that is,

$$L(\boldsymbol{x}) = \boldsymbol{\vartheta}^{*T}\boldsymbol{\beta}_1(\boldsymbol{x}) + \varepsilon \tag{38}$$

where $\varepsilon \in R^n$ is the approximation error satisfying $|\varepsilon| \leq \bar{\varepsilon}'$, $\boldsymbol{\vartheta}^* \in R^\ell$ is the ideal weight vector and $\boldsymbol{\beta}_1(\boldsymbol{x}) \in R^\ell$ is the basis function vector. Then, taking the following transformation for $\bar{\boldsymbol{f}}(\boldsymbol{Z})$ yields

$$\begin{aligned}||\bar{\boldsymbol{f}}(\boldsymbol{Z})|| &\leq L(\boldsymbol{x}) + ||\boldsymbol{d_x} - \ddot{\boldsymbol{x}}_{\boldsymbol{d}}|| + ||\breve{\boldsymbol{\psi}}(\boldsymbol{e_1})\boldsymbol{e_2}|| \\ &\leq ||\boldsymbol{\vartheta}^*||||\boldsymbol{\beta}_1(\boldsymbol{x})|| + \bar{\varepsilon}' + ||\boldsymbol{d_x} - \ddot{\boldsymbol{x}}_{\boldsymbol{d}}|| + ||\breve{\boldsymbol{\psi}}(\boldsymbol{e_1})\boldsymbol{e_2}|| \\ &\leq \theta\bar{\varsigma}(\boldsymbol{Z})\end{aligned} \tag{39}$$

where $\bar{\varsigma}(\boldsymbol{Z}) = ||\boldsymbol{\beta}_1(\boldsymbol{x})|| + ||\breve{\boldsymbol{\psi}}(\boldsymbol{e_1})\boldsymbol{e_2}|| + 1$ and $\theta = \max\{||\boldsymbol{\vartheta}^*||, \bar{\varepsilon}' + ||\boldsymbol{d_x} - \ddot{\boldsymbol{x}}_{\boldsymbol{d}}||, 1\}$.

Remark 5: According to (25) and (38), the main difference between them is that only one RBF NN is employed to handle the unknown nonlinear function $\boldsymbol{f}(\boldsymbol{x})$ in the subsection B (indirect approximation method). Obviously, such an operation in this subsection can reduce the number of neurons such that the computational burden is decreased.

Recalling Eqs. (23) and (26), one has

$$\boldsymbol{\chi}^T\dot{\boldsymbol{\chi}} \leq \boldsymbol{\chi}^T\boldsymbol{g}(\boldsymbol{x})\boldsymbol{\varrho}\boldsymbol{\tau}_c + \theta||\boldsymbol{\chi}||\bar{\varsigma}(\boldsymbol{Z}) \tag{40}$$

Design the control law for ELSs (1) as follows

$$\boldsymbol{\tau}_c = N(\boldsymbol{\zeta})\bar{\eta}\boldsymbol{\chi} \tag{41}$$

$$\dot{\zeta} = \boldsymbol{\chi}^T\boldsymbol{\chi}\bar{\eta} \tag{42}$$

$$\bar{\eta} = k_1 + \hat{\theta}\bar{\varsigma}^2(\boldsymbol{Z}) \tag{43}$$

$$\dot{\hat{\theta}} = \bar{\rho}\boldsymbol{\chi}^T\boldsymbol{\chi}\bar{\varsigma}^2(\boldsymbol{Z}) - \bar{\sigma}\hat{\theta} \tag{44}$$

where $k_1 > 0$, $\bar{\rho} > 0$ and $\bar{\sigma} > 0$ are design constants and ζ is the Nussbaum variable.

Consider the following Lyapunov function

$$V_1 = \frac{1}{2}\boldsymbol{\chi}^T\boldsymbol{\chi} + \frac{1}{2\bar{\rho}}\tilde{\theta}^2 \tag{45}$$

Taking the time-derivative of V_1, and using Eqs. (18), (40) and (41), one can obtain

$$\begin{aligned}\dot{V}_1 &\leq N(\zeta)\bar{\eta}\boldsymbol{\chi}^T\boldsymbol{g}(\boldsymbol{x})\boldsymbol{\varrho}\boldsymbol{\chi} + \boldsymbol{\chi}^T\theta\boldsymbol{\chi}\bar{\varsigma}^2(\boldsymbol{Z}) + \frac{\theta+1}{4} - \frac{1}{\bar{\rho}}\tilde{\theta}\dot{\hat{\theta}} \\ &\leq \Big(N(\zeta)a(t) + 1\Big)\dot{\zeta} - k_1\boldsymbol{\chi}^T\boldsymbol{\chi} - \frac{\bar{\sigma}}{2\bar{\rho}}\tilde{\theta}^2 + \frac{\bar{\sigma}}{2\bar{\rho}}\theta^2 + \frac{\theta+1}{4} \\ &= -c_1V_1 + \Big(N(\zeta)a(t) + 1\Big)\dot{\zeta} + d_1\end{aligned} \tag{46}$$

where $c_1 = \min\{2k_1, \bar{\sigma}\}$ and $d_1 = \frac{\bar{\sigma}}{2\bar{\rho}}\theta^2 + \frac{\theta+1}{4}$.

The main results are given by the following theorem.

Theorem 2: Consider the uncertain ELSs (1) under Assumptions 1-3, if the initial condition of q satisfies $|q_{1,i}(0)| < \kappa_{c,i}$ for $\forall i$, then the designed control law (41) with the adaptive laws (42) and (44) is able to make the following properties hold

1) All signals in the closed-loop tracking control system are uniformly bounded.
2) The output $\boldsymbol{q}$ of ELSs (1) will never violate the output constraint condition, i.e., $|q_{1,i}| < \kappa_{c,i}, \forall i \in \{1, \cdots, n\}$.

Zero-error

3) tracking control is achieved, i.e., $\boldsymbol{e_1} \to 0$ as $t \to 0$.

Proof: The proof of Theorem 2 can follow the same approach as Theorem 1.

IV. SIMULATION

To verify the effectiveness of the proposed neuroadaptive control schemes, a two-link RM and its dynamics described by (1) is given as followings

$$\boldsymbol{M}(\boldsymbol{q}) = \begin{bmatrix} m_1l_1^2 + m_2\Lambda + \mu_1 + \mu_2 & m^* \\ m^* & m_2l_2^2 + \Pi_2 \end{bmatrix} \tag{47}$$

$$\boldsymbol{C}(\boldsymbol{q}, \dot{\boldsymbol{q}}) = -m_2L_1l_2\sin(q_2)\begin{bmatrix} \dot{q}_2 & \dot{q}_1 + \dot{q}_2 \\ -\dot{q}_1 & 0 \end{bmatrix} \tag{48}$$

$$\boldsymbol{G}(\boldsymbol{q}) = \begin{bmatrix} (m_1l_1 + m_2L_1)g\cos(q_1) + m_2l_2g\cos(q_1 + q_2) \\ m_2l_2\cos(q_1 + q_2) \end{bmatrix} \tag{49}$$

$$\boldsymbol{F}(\boldsymbol{q}, \dot{\boldsymbol{q}}) = 0.5\begin{bmatrix} \tanh(\dot{q}_1) \\ \tanh(q_2)\cos(q_1 + q_2) \end{bmatrix} \tag{50}$$

$$\boldsymbol{\tau_d} = 0.25\begin{bmatrix} \cos(0.1\pi t)\sin(0.5t) \\ 0.5\sin(0.15t)\sin(t/3)\cos(0.02t) \end{bmatrix} + \boldsymbol{\tau_\varpi} \tag{51}$$

where m_i, L_i and ϑ_i denote the mass, length and inertia moment of the ith link, respectively; l_i denotes the distance from the base of the ith link to its center of mass, and g denotes the gravitation constant. $m^* = m_2(l_2^2) + L_1l_2\cos(q_2) + \vartheta_2$ and $\Lambda = L_1^2 + l_2^2 + 2L_1l_2(l_2 + \cos(q_2))$. In simulation, $m_1 = 1.6kg$, $m_2 = 0.8kg$, $L_1 = 0.4m$, $L_2 = 0.3m$, $l_1 = 0.25m$, $l_2 = 0.15m$, $\mu_1 = 0.0853kg \cdot m^2$, $\mu_2 = 0.024kg \cdot m^2$ and

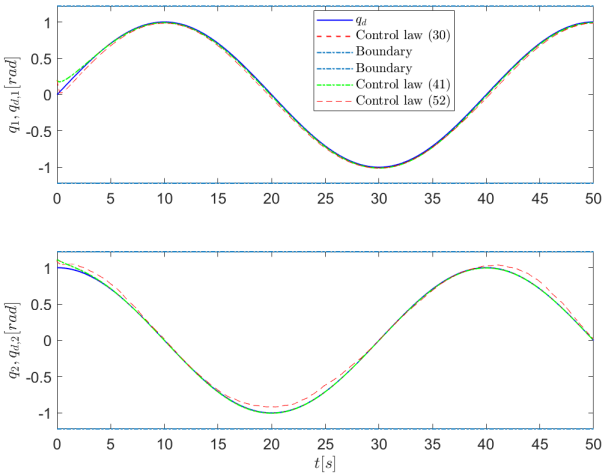

FIGURE 1. Tracking performance.

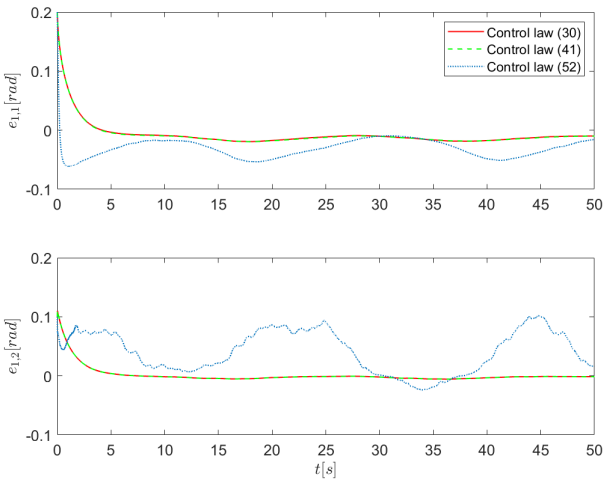

FIGURE 2. Tracking error.

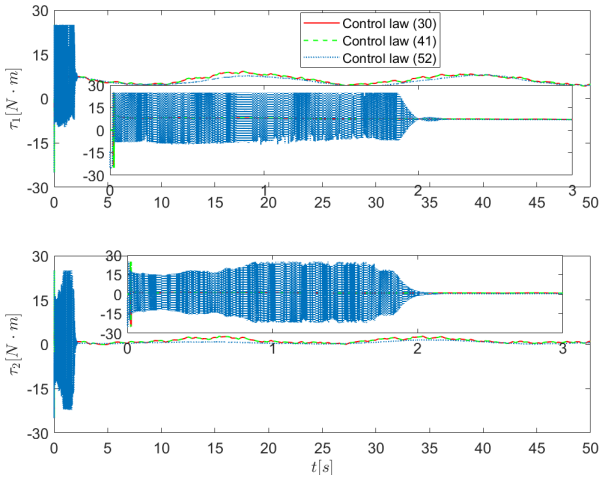

FIGURE 3. Control input.

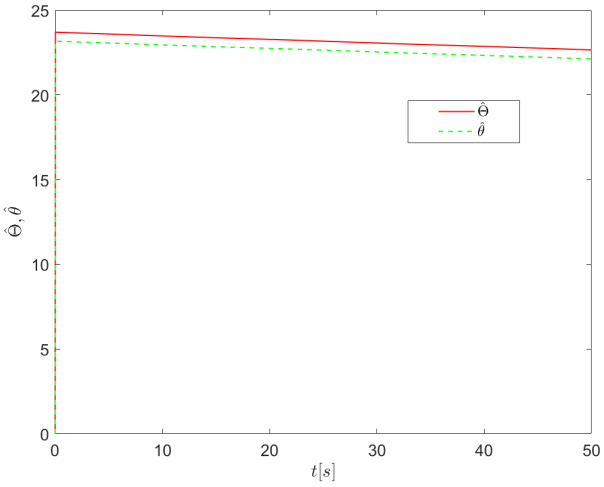

FIGURE 4. 2-norms of $\hat{\theta}$ and $\hat{\Theta}$.

$g = 9.81\ m/s$. $\dot{\tau}_{\varpi,i} + \tau_{\varpi,i} = \nu_i \varpi$, where ϖ is the Gaussian white noise (GWN) and ν_i is the amplitude of GWN.

In simulation, the desired trajectory is set as $\boldsymbol{q_d} = [\sin(0.05\pi t); \cos(0.05\pi t)]$. The saturation limits are given by $\tau_{i,m} = 25(N \cdot m)$, $i = 1, 2$. The initial states are $\boldsymbol{q}(0) = [0.2rad, 1.1rad]^T$, $\dot{\boldsymbol{q}}(0) = [0, 0]^T$, $\zeta(0) = 0.1$, $\varpi(0) = 0$ and $\hat{\theta}(0) = \hat{\Theta} = 0$. The design parameters are selected as $k = k_1 = 16$, $k_{c,1} = 1.22$, $k_{c,2} = -1.22$, $\rho = \bar{\rho} = 2$, $\sigma = \bar{\sigma} = 0.01$, $\nu_1 = 1.2$, $\nu_2 = 1.0$ and $\delta_i = 0.3$. The RBF NNs for $\varphi(Z)$ contain 20 nodes with the centers evenly spaced in the range $[-2, 2] \times \ddot{4} \times [-2, 2]$ and the widths $\sigma_j = 2\ (j = 1, \cdots, 20)$.

The simulation results under our proposed two neuroadaptive control schemes are presented in Figs. 1-5, respectively. Fig. 1 presents the tracking control results under the direct/indirect neuroadaptive control law, which implies that the direct/indirect neuroadaptive control law can force the output $\boldsymbol{q}$ of RM to track $\boldsymbol{q_d}$ with satisfactory performance and the output $\boldsymbol{q}$ does not violate the constraint boundaries. Fig. 2 give the curves of tracking errors $\boldsymbol{e_1}$ and the results indicates that the designed control law can force the tracking error $e_{1,i}$ converges to zero as $t \to \infty$, i.e., $e_{1,i} \to 0$ as $t \to \infty$. Fig. 3 shows the curve of control input $\boldsymbol{\tau}$, which are bounded and reasonable. The estimation values $\hat{\Theta}$ and $\hat{\theta}$ are drawn in Fig. 4, which implied that $\hat{\Theta}$ and $\hat{\theta}$ are bounded. Fig. 5 shows that the Nussbaum function $N(\zeta)$ and its variable ζ are bounded. The simulation results indicate that all signals in the closed-loop tracking control system under our proposed schemes are bounded, and the tracking error $\boldsymbol{e_1}$ converges to zero.

In addition, to further analyze the difference between the direct and indirect neuroadaptive control laws, the performance indices on the tracking error $\boldsymbol{e_1}$ and the control input $\boldsymbol{\tau}$ are summarized in Table 1, where IAE $= \int_0^{t_l} |e_{1,i}| dt$ denotes the integrated absolute error and MIAC $= \frac{1}{t_l - 0} \int_0^{t_l} |\tau_i| dt$ denotes the mean integrated absolute control. From the index of IAE, the control accuracy of the direct and indirect neuroadaptive control law is basically the same, which indicates that the number of NN do not affected the control accuracy. In addition, the index of MIAC under the two control laws is also the same. Therefore, the quantitative indicators IAE and IMAC show that the proposed indirect neuroadaptive control

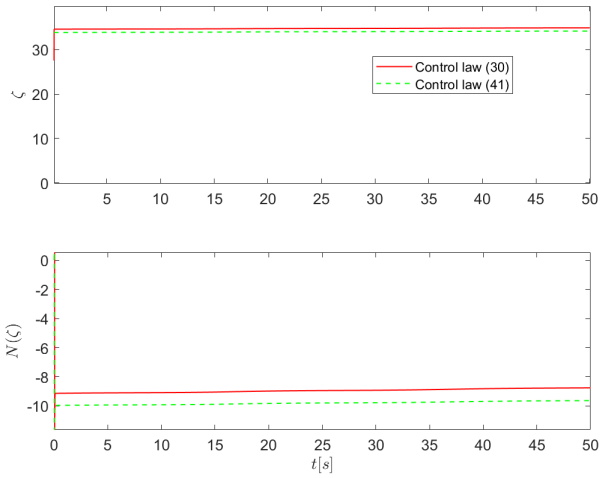

FIGURE 5. Settling time comparison between three schemes.

scheme not only can ensure the control performance, but also can reduce the computational load of control algorithm. Hence, the simulation and quantitative results demonstrate the desirable features of the proposed control scheme as proved Theorem 1.

To illuminate the superiority of our proposed direct/indirect neuroadaptive control scheme, simulation comparisons with the finite-time terminal SMC scheme proposed in [20] is carried out. In simulation, the design parameters of the finite-time terminal SMC law are same with those in [20], and the initial states $\theta(0)$ and $\dot{\theta}(0)$ are identical to the counterparts for the simulations under our proposed tracking control schemes. The finite-time terminal SMC law is given by

$$\boldsymbol{\tau}_{sm} = -\boldsymbol{A}\boldsymbol{S}^{h} - \hat{\boldsymbol{\vartheta}}^{T}\boldsymbol{\beta}(\boldsymbol{x}) - \boldsymbol{u}_{\delta} \tag{52}$$

$$\dot{\hat{\boldsymbol{\vartheta}}} = \boldsymbol{\Phi}\boldsymbol{\beta}(\boldsymbol{x})\boldsymbol{S}^{T} \tag{53}$$

$$\boldsymbol{u}_{\delta} = \begin{cases} \dfrac{(\upsilon + \bar{\upsilon})\boldsymbol{S}}{||\boldsymbol{S}||} \\ \boldsymbol{0} \end{cases} \tag{54}$$

TABLE 1. Performance comparison.

Index	Items	Control law (30)	Control law (40)
IAE	$e_{1,1}$	0.782	0.7948
	$e_{1,2}$	0.2697	0.2704
MIAC	τ_1	6.54	1.163
	τ_2	6.552	1.634

The simulation results under the SMC schemes are plotted using dotted line in Figs. 1-3, respectively. It is obvious from Fig.1 that the SMC scheme can also force the output $\boldsymbol{q}$ of RM to track $\boldsymbol{q_d}$. From Fig. 2, the SMC law exhibits the fast response performance, but the tracking control accuracy is poorer than that of our proposed control schemes. In addition, it can be clearly seen form Fig. 3 that there exists severe chattering in the curve of control input $\boldsymbol{\tau}$. Therefore, the simulation comparisons further show that the proposed direct/indirect neuroadaptive control schemes are effective and the computation is inexpensive, meanwhile the control accuracy can also be ensured.

To verify that the output constraint capability of the proposed control schemes, simulation comparisons are carried out with the direct/indirect approximation method without output constraint. From (19), if the output constraint is not considered in the control design, the variable $\boldsymbol{\chi}$ can be written as $\boldsymbol{\chi} = \boldsymbol{e_2} + \boldsymbol{\delta e_1}$ with $\boldsymbol{\delta} = diag(\delta_1, \delta_2)$. For the direct/indirect approximation method without output constraint (DAMWOOC/IAMWOOC), the structure of control law is the same as that one in this work. In addition, the design parameters on the control laws without output constraint are identical to the counterparts for the control laws (30) and (41). The simulation results are shown in Fig. 6, from which we can find that the output q_i $(i = 1, 2)$ under DAMWOOC/IAMWOOC violates the constraint boundary, which show that the output constraint capability of the proposed control schemes is verified.

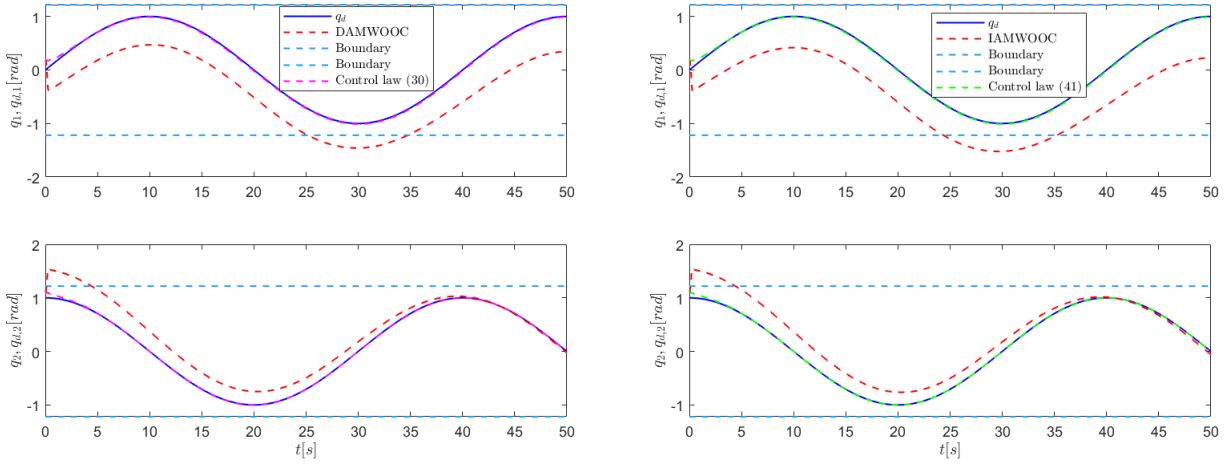

(a) (b)

FIGURE 6. Simulation comparison results.

V. CONCLUSION

In this paper, we have addressed the neuroadaptive tracking control problem for ELSs in the simultaneous presence of uncertain dynamics, unknown disturbances and constraints both in input saturation. The direct/indirect adaptive NN and virtual-parameter learning method are taken into the control design to handle the internal and external uncertainties. In addition, the Gaussian error function is applied to replace the non-smooth input saturation nonlinearity. And then, the Nussbaum function technology is used to solve the time-varying gain issue cause by the Gaussian error function. The theoretical analysis indicates that under the proposed direct/indirect neuroadaptive tracking control schemes, all signals in the closed-loop Euler-Lagrange tracking control system are bounded and the zero tracking error is achieved. The simulation results show that the tracking control is reached with zero tracking error. In the further, we will investigate the zero tracking control issue under the event-triggered mechanism.

APPENDIX A
PROOF OF LEMMA 6

For any z satisfies $|z| < \kappa$, the item $\left(\frac{\kappa z}{\kappa^2 - z^2}\right)^2$ in Eq. (14) can be rewritten as

$$\left(\frac{\kappa z}{\kappa^2 - z^2}\right)^2 = \log\left(\exp\left(\frac{\kappa z}{\kappa^2 - z^2}\right)^2\right) \tag{55}$$

Using Taylor expansion, Eq.(55) can be rewritten as

$$\begin{aligned}\left(\frac{\kappa z}{\kappa^2 - z^2}\right)^2 &= \log\left(1 + \left(\frac{\kappa z}{\kappa^2 - z^2}\right)^2 + \sum_{n=2}^{\infty} \frac{\left(\left(\frac{\kappa z}{\kappa^2 - z^2}\right)^2\right)^n}{n!}\right) \\ &\geq \log\left(1 + \left(\frac{\kappa z}{\kappa^2 - z^2}\right)^2\right) \\ &\geq \log\left(\frac{\kappa^4}{\left(\kappa^2 - z^2\right)^2}\right) \\ &= 2\log\left(\frac{\kappa^2}{\kappa^2 - z^2}\right)\end{aligned} \tag{56}$$

Therefore, Lemma 6 is proved.

APPENDIX B
PROOF OF LEMMA 7

Consider the Lyapunov function as follows

$$V_{\boldsymbol{e}} = \frac{1}{2}\sum_{i=1}^{n} \log\left(\frac{\kappa_i^2}{\kappa_i^2 - e_{1,i}^2}\right) \tag{57}$$

The time-derivative of $V_{\boldsymbol{e}}$ is

$$\dot{V}_{\boldsymbol{e}} = \sum_{i=1}^{n} \frac{e_{1,i}\dot{e}_{1,i}}{\kappa_i^2 - e_{1,i}^2} = \boldsymbol{e_1}^T \bar{\boldsymbol{\psi}}(\boldsymbol{e_1})\dot{\boldsymbol{e}}_{\boldsymbol{1}} \tag{58}$$

where $\bar{\boldsymbol{\psi}}(\boldsymbol{e_1}) = diag(\frac{1}{\kappa_1^2 - e_{1,1}^2}, \cdots, \frac{1}{\kappa_n^2 - e_{1,n}^2})$.

From $\boldsymbol{e_2} = \dot{\boldsymbol{e}}_{\boldsymbol{1}}$, Eq.(19) and Lemma 4, one can get

$$\begin{aligned}\dot{V}_{\boldsymbol{e}} &= \boldsymbol{e_1}^T \bar{\boldsymbol{\psi}}(\boldsymbol{e_1})\left(\boldsymbol{\chi} - \boldsymbol{\psi}(\boldsymbol{e_1})\boldsymbol{e_1}\right) \\ &\leq -\boldsymbol{e_1}^T \bar{\boldsymbol{\psi}}(\boldsymbol{e_1})\boldsymbol{\psi}(\boldsymbol{e_1})\boldsymbol{e_1} + \boldsymbol{e_1}^T \bar{\boldsymbol{\psi}}^2(\boldsymbol{e_1})\boldsymbol{e_1} + \frac{\boldsymbol{\chi}^T\boldsymbol{\chi}}{4} \\ &= -\sum_{i=1}^{n} \frac{(\delta_i - 1)e_{1,i}^2}{(\kappa_i^2 - e_{1,i}^2)^2} + \frac{\boldsymbol{\chi}^T\boldsymbol{\chi}}{4} \\ &= -\sum_{i=1}^{n} \frac{\delta_i - 1}{\kappa_i^2}\left(\frac{\kappa_i e_{1,i}}{\kappa_i^2 - e_{1,i}^2}\right)^2 + \frac{\boldsymbol{\chi}^T\boldsymbol{\chi}}{4}\end{aligned} \tag{59}$$

Further, using Lemma 5, Eq.(59) can be rewritten as

$$\begin{aligned}\dot{V}_{\boldsymbol{e}} &\leq -2\sum_{i=1}^{n}\left[\frac{\delta_i - 1}{\kappa_i^2}\log\left(\frac{\kappa_i^2}{\kappa_i^2 - e_{1,i}^2}\right)\right] + \frac{\boldsymbol{\chi}^T\boldsymbol{\chi}}{4} \\ &\leq -4\rho V_{\boldsymbol{e}} + \frac{\boldsymbol{\chi}^T\boldsymbol{\chi}}{4}\end{aligned} \tag{60}$$

where $\rho = \min\{\frac{\delta_i - 1}{\kappa_i^2}, i = 1, \cdots, n\}$ with $\delta_i > 1$.

From Eq.(60), if $|q_{1,i}(0)| < \kappa_{c,i}$ holds $\forall i$ and $\boldsymbol{\chi}$ is bounded for $\forall t \geq 0$, then $V_{\boldsymbol{e}}$ is bounded. Further, $\boldsymbol{e_1}$ is also bounded and $|e_{1,i}| < \kappa_i$, that is, $|x_{1,i} - x_{d,i}| < \kappa_i$. Considering Assumption 3, on can obtain

$$-\kappa_i - k_{d,i} \leq -\kappa_i + x_{d,i} < x_{1,i} < \kappa_i + x_{d,i} \leq \kappa_i + k_{d,i} \tag{61}$$

Recalling Eq.(20), we have $-\kappa_{c,i} < x_{1,i} < \kappa_{c,i}$, that is, $|q_{1,i}| < \kappa_{c,i}$ always holds. Therefore, Lemma 7 is proved.

REFERENCES

[1] G. Zhu, Y. Ma, and S. Hu, "Single-parameter-learning-based finite-time tracking control of underactuated MSVs under input saturation," *Control Eng. Pract.*, vol. 105, Dec. 2020, Art. no. 104652.
[2] Y. Ma, Z. Nie, S. Hu, Z. Li, R. Malekian, and M. Sotelo, "Fault detection filter and controller co-design for unmanned surface vehicles under DoS attacks," *IEEE Trans. Intell. Transp. Syst.*, vol. 22, no. 3, pp. 1422–1434, Mar. 2021, doi: 10.1109/TITS.2020.2970472.
[3] G. Zhu and J. Du, "Robust adaptive neural practical fixed-time tracking control for uncertain Euler–Lagrange systems under input saturations," *Neurocomputing*, vol. 412, pp. 502–513, Oct. 2020.
[4] K. Zhao, Y. Song, T. Ma, and L. He, "Prescribed performance control of uncertain Euler–Lagrange systems subject to full-state constraints," *IEEE Trans. Neural Netw. Learn. Syst.*, vol. 29, no. 8, pp. 3478–3489, Aug. 2018.
[5] C. Wei, J. Luo, C. Ma, H. Dai, and J. Yuan, "Event-triggered neuroadaptive control for postcapture spacecraft with ultralow-frequency actuator updates," *Neurocomputing*, vol. 315, pp. 310–321, Nov. 2018.
[6] N. Sarkar, T. K. Podder, and G. Antonelli, "Fault-accommodating thruster force allocation of an AUV considering thruster redundancy and saturation," *IEEE Trans. Robot. Autom.*, vol. 18, no. 2, pp. 223–233, Apr. 2002.
[7] R. Cui, L. Chen, C. Yang, and M. Chen, "Extended state observer-based integral sliding mode control for an underwater robot with unknown disturbances and uncertain nonlinearities," *IEEE Trans. Ind. Electron.*, vol. 64, no. 8, pp. 6785–6795, Aug. 2017.
[8] H. G. Sage, M. F. De Mathelin, and E. Ostertag, "Robust control of robot manipulators: A survey," *Int. J. Control*, vol. 72, no. 16, pp. 1498–1522, Jan. 1999.
[9] S. Liuzzo and P. Tomei, "A global adaptive learning control for robotic manipulators," *Automatica*, vol. 44, no. 5, pp. 1379–1384, May 2008.
[10] L. Bascetta and P. Rocco, "Revising the robust-control design for rigid robot manipulators," *IEEE Trans. Robot.*, vol. 26, no. 1, pp. 180–187, Feb. 2010.
[11] C. Chen, G. Zhu, Q. Zhang, and J. Zhang, "Robust adaptive finite-time tracking control for uncertain Euler–Lagrange systems with input saturation," *IEEE Access*, vol. 8, pp. 187605–187614, Oct. 2020.

[12] S. Roy, S. B. Roy, and I. N. Kar, "Adaptive–robust control of Euler–Lagrange systems with linearly parametrizable uncertainty bound," *IEEE Trans. Control Syst. Technol.*, vol. 26, no. 5, pp. 1842–1850, Sep. 2018.
[13] N. Sadegh and R. Horowitz, "An exponentially stable adaptive control law for robot manipulators," *IEEE Trans. Robot. Autom.*, vol. 6, no. 4, pp. 491–496, Aug. 1990.
[14] Y. Pan and H. Yu, "Composite learning robot control with guaranteed parameter convergence," *Automatica*, vol. 89, pp. 398–406, Mar. 2018.
[15] W. Deng and J. Yao, "Extended-state-observer-based adaptive control of electrohydraulic servomechanisms without velocity measurement," *IEEE/ASME Trans. Mechatronics*, vol. 25, no. 3, pp. 1151–1161, Jun. 2020.
[16] A. R. Pereira, L. Hsu, and R. Ortega, "Globally stable adaptive formation control of Euler–Lagrange agents via potential functions," in *Proc. Amer. Control Conf.*, St. Louis, MO, USA, 2009, pp. 2606–2611.
[17] S. Islam and X. P. Liu, "Robust sliding mode control for robot manipulators," *IEEE Trans. Ind. Electron.*, vol. 58, no. 6, pp. 2444–2453, Jun. 2011.
[18] W. Deng and J. Yao, "Asymptotic tracking control of mechanical servosystems with mismatched uncertainties," *IEEE/ASME Trans. Mechatronics*, early access, Oct. 30, 2020, doi: 10.1109/TMECH.2020.3034923.
[19] S. S. Ge, C. C. Hang, and L. C. Woon, "Adaptive neural network control of robot manipulators in task space," *IEEE Trans. Ind. Electron.*, vol. 44, no. 6, pp. 746–752, Dec. 1997.
[20] L. Wang, T. Chai, and L. Zhai, "Neural-network-based terminal sliding-mode control of robotic manipulators including actuator dynamics," *IEEE Trans. Ind. Electron.*, vol. 56, no. 9, pp. 3296–3304, Sep. 2009.
[21] W. He, A. O. David, Z. Yin, and C. Sun, "Neural network control of a robotic manipulator with input deadzone and output constraint," *IEEE Trans. Syst., Man, Cybern. Syst.*, vol. 46, no. 6, pp. 759–770, Jun. 2016.
[22] S. Zhang, Y. Dong, Y. Ouyang, Z. Yin, and K. Peng, "Adaptive neural control for robotic manipulators with output constraints and uncertainties," *IEEE Trans. Neural Netw. Learn. Syst.*, vol. 29, no. 11, pp. 5554–5564, Nov. 2018, doi: 10.1109/TNNLS.2018.2803827.
[23] Y.-J. Liu, S. Lu, and S. Tong, "Neural network controller design for an uncertain robot with time-varying output constraint," *IEEE Trans. Syst., Man, Cybern. Syst.*, vol. 47, no. 8, pp. 2060–2068, Aug. 2017.
[24] W. He, H. Huang, and S. S. Ge, "Adaptive neural network control of a robotic manipulator with time-varying output constraints," *IEEE Trans. Cybern.*, vol. 47, no. 10, pp. 3136–3147, Oct. 2017.
[25] Z. Zhao, W. He, and S. S. Ge, "Adaptive neural network control of a fully actuated marine surface vessel with multiple output constraints," *IEEE Trans. Control Syst. Technol.*, vol. 22, no. 4, pp. 1536–1543, Jul. 2014.
[26] X. Jin, "Fault tolerant finite-time leader–follower formation control for autonomous surface vessels with LOS range and angle constraints," *Automatica*,vol. 68, pp. 228–236, Jun. 2016.
[27] Z. Zhang and Y. Wu, "Adaptive fuzzy tracking control of autonomous underwater vehicles with output constraints," *IEEE Trans. Fuzzy Syst.*, early access, Jan. 17, 2020, doi: 10.1109/TFUZZ.2020.2967294.
[28] J.-X. Zhang and G.-H. Yang, "Fault-tolerant output-constrained control of unknown Euler–Lagrange systems with prescribed tracking accuracy," *Automatica*, vol. 111, Jan. 2020, Art. no. 108606.
[29] J. Wang, P. Wang, and X. Ma, "Adaptive event-triggered control for quadrotor aircraft with output constraints," *Aerosp. Sci. Technol.*, vol. 105, Oct. 2020, Art. no. 105935.
[30] W. He, Z. Yin, and C. Sun, "Adaptive neural network control of a vessel with output constraints using the asymmetric Barrier Lyapunov function," *IEEE Trans. Cybern.*, vol. 47, no. 7, pp. 1641–1651, Jul. 2017.
[31] Y. Su and J. Swevers, "Finite-time tracking control for robot manipulators with actuator saturation," *Robot. Comput.-Integr. Manuf.*, vol. 30, no. 2, pp. 91–98, Apr. 2014.
[32] W. He, Y. Dong, and C. Sun, "Adaptive neural impedance control of a robotic manipulator with input saturation," *IEEE Trans. Syst., Man, Cybern. Syst.*, vol. 46, no. 3, pp. 334–344, Mar. 2016.
[33] M. Li, Y. Li, S. S. Ge, and T. H. Lee, "Adaptive control of robotic manipulators with unified motion constraints," *IEEE Trans. Syst., Man, Cybern. Syst.*, vol. 47, no. 1, pp. 184–194, Jan. 2017.
[34] E. Arefinia, H. A. Talebi, and A. Doustmohammadi, "A robust adaptive model reference impedance control of a robotic manipulator with actuator saturation," *IEEE Trans. Syst., Man, Cybern. Syst.*, vol. 50, no. 2, pp. 409–420, Feb. 2020.
[35] X. Hu, X. Wei, H. Zhang, J. Han, and X. Liu, "Robust adaptive tracking control for a class of mechanical systems with unknown disturbances under actuator saturation," *Int. J. Robust Nonlinear Control*, vol. 29, no. 6, pp. 1893–1908, Apr. 2019.
[36] Y. Ma, G. Zhu, and Z. Li, "Error-driven-based nonlinear feedback recursive design for adaptive NN trajectory tracking control of surface ships with input saturation," *IEEE Intell. Transp. Syst. Mag.*, vol. 11, no. 2, pp. 17–28, Summer 2019.
[37] G. Zhu and J. Du, "Global robust adaptive trajectory tracking control for surface ships under input saturation," *IEEE J. Ocean. Eng.*, vol. 45, no. 2, pp. 442–450, Apr. 2020.
[38] X. He, Z. Zhao, and Y. Song, "Active control for flexible mechanical systems with mixed deadzone-saturation input nonlinearities and output constraint," *J. Franklin Inst.*, vol. 356, no. 9, pp. 4749–4772, Jun. 2019.
[39] H. Hu, B. Wang, Z. Cheng, L. Liu, Y. Wang, and X. Luo, "A novel active fault-tolerant control for spacecrafts with full state constraints and input saturation," *Aerosp. Sci. Technol.*, vol. 108, Jan. 2021, Art. no. 106368.
[40] J.-G. Sun, C.-M. Li, Y. Guo, C.-Q. Wang, and P. Li, "Adaptive fault tolerant control for hypersonic vehicle with input saturation and state constraints," *Acta Astronautica*, vol. 167, pp. 302–313, Feb. 2020.
[41] Z. Zheng, Y. Huang, L. Xie, and B. Zhu, "Adaptive trajectory tracking control of a fully actuated surface vessel with asymmetrically constrained input and output," *IEEE Trans. Control Syst. Technol.*, vol. 26, no. 5, pp. 1851–1859, Sep. 2018.
[42] H. Qin, C. Li, Y. Sun, X. Li, Y. Du, and Z. Deng, "Finite-time trajectory tracking control of unmanned surface vessel with error constraints and input saturations," *J. Franklin Inst.*, vol. 357, no. 16, pp. 11472–11495, Nov. 2020, doi: 10.1016/j.jfranklin.2019.07.019.
[43] G. Zhu, J. Du, and Y. Kao, "Robust adaptive neural trajectory tracking control of surface vessels under input and output constraints," *J. Franklin Inst.*, vol. 357, no. 13, pp. 8591–8610, Sep. 2020.
[44] D. Wang and M. Fu, "Adaptive formation control for waterjet USV with input and output constraints based on bioinspired neurodynamics," *IEEE Access*, vol. 7, pp. 165852–165861, Nov. 2019.
[45] A. Zahaf, S. Bououden, M. Chadli, and M. Chemachema, "Robust fault tolerant optimal predictive control of hybrid actuators with time varying delay for industrial robot arm," *Asian J. Control*, pp. 1–15, Oct. 2020, doi: 10.1002/asjc.2444.
[46] G. Zhu, J. Du, J. Li, and Y. Kao, "Robust adaptive NN tracking control for MIMO uncertain nonlinear systems with completely unknown control gains under input saturations," *Neurocomputing*, vol. 365, pp. 125–136, Nov. 2019.
[47] T. Zhang and S. S. Ge, "Adaptive neural network tracking control of MIMO nonlinear systems with unknown dead zones and control directions," *IEEE Trans. Neural Netw.*, vol. 20, no. 3, pp. 483–497, Mar. 2009.
[48] W. Shi, "Adaptive fuzzy control for MIMO nonlinear systems with non-symmetric control gain matrix and unknown control direction," *IEEE Trans. Fuzzy Syst.*, vol. 22, no. 5, pp. 1288–1300, Oct. 2014.
[49] J. E. Slotine and W. Li, *Applied Nonlinear Control*. Englewood Cliffs, NJ, USA: Prentice-Hall, 1991.
[50] H. Deng and M. Krstić, "Stochastic nonlinear stabilization—I: A backstepping design," *Syst. Control Lett.*, vol. 32, no. 3, pp. 143–150. Nov. 1997.